Available online at www.sciencedirect.com
SCIENCE DIRECT®
International Journal of Multiphase Flow 30 (2004) 1311–1336
International Journal of Multiphase Flow
www.elsevier.com/locate/ijmulflow

Concentration profiles in a turbulent suspension when gravity is not affecting deposition

Yoichi Mito, Thomas J. Hanratty *

Department of Chemical and Biomolecular Engineering, University of Illinois, 205 Roger Adams Laboratory, Box C-3, 600 South Mathews Avenue, Urbana, IL 61801, USA

Received 4 February 2004; received in revised form 17 August 2004

Abstract

An idealized representation of the dispersed flow in a fully-developed annular pattern is considered for the case of zero gravitational effects. The walls of a two-dimensional channel are represented as presenting arrays of infinitesimal particle sources. The behavior of a single source is described by modeling the fluid turbulence seen by the particles with a modified Langevin equation. By carrying out the calculations over a wide range of dimensionless time constants the deposition process could be followed, as the controlling mechanism changed from Brownian diffusion, to turbulent diffusion, to free-flight, to unidirectional non-turbulent trajectories. The calculation of local mean particle accelerations allowed a direct evaluation of the turbophoretic velocity. A consideration of the concentration profiles indicates that a Boussinesq representation of turbulent mixing is not valid in an Eulerian analysis.

Keywords: Disperse flow; Concentration profiles; Turbophoresis; Particle deposition; Stochastic analysis; Langevin equation

* Corresponding author. Tel.: +1 217 333 1318; fax: +1 217 333 5052.
E-mail address: hanratty@scs.uiuc.edu (T.J. Hanratty).

0301-9322/$ - see front matter © 2004 Elsevier Ltd. All rights reserved.
doi:10.1016/j.ijmultiphaseflow.2004.08.003

1. Introduction

Understanding of dispersion and deposition of particles in a turbulent field has been advanced through studies of the behavior of point sources in direct numerical simulations (DNS). The difficulty with this approach is that computer requirements limit studies to small Reynolds numbers, small durations and to a range of variables that is insufficient to capture, completely, the physics. Therefore, we have explored the use of a stochastic method which uses a modified Langevin equation (Mito and Hanratty, 2002; Iliopoulos et al., 2003) to represent the fluid turbulence. This approach has been tested at $Re_\tau = Hv^*/\nu = 150$, where H is the half height of the channel, v^*, the friction velocity and ν, the kinematic viscosity, by considering sources of tracers located in the fluid (Iliopoulos et al., 2003) and at the wall (Mito and Hanratty, 2003).

The success of these comparisons prompted a comprehensive study of an idealized version of an annular flow in a horizontal rectangular channel. The concentration field of drops in an annular flow is pictured as resulting from a distribution of sources on the films flowing along the walls. Drops, which are represented by spherical solid particles, are injected from both walls and eventually deposit on the walls. At sufficiently large computation times, a fully-developed condition is realized, for which the rates of injection and deposition are equal and the concentration field is not changing (Binder and Hanratty, 1992). It is noted that this system differs from previous calculations of deposition which used a uniform distribution of particles as the initial condition and allowed the number of particles in the field to change with time. Calculations were done over a range of dimensionless inertial time constants of $\tau_p^+ = \tau_p v^{*2}/\nu = 3$–40, and dimensionless terminal velocities of $V_T^+ = 0$–3.2.

Results for the effect of gravity on the rate of deposition are given in a previous paper by Mito and Hanratty (2004). This paper presents calculations of the concentration profiles and a more detailed examination of the deposition process for $V_T = 0$ (zero gravity). This is essentially the same as a vertical flow if lift forces are neglected. Early work by Friedlander and Johnstone (1957) and others used the assumption that the concentration would be close to zero at a perfectly absorbing wall. Particles were pictured to move toward the wall by turbulent dispersion and to deposit by free-flight from a fixed location in the fluid. Lee et al. (1989) have argued that, for free-flights, the particle concentration at the wall would be finite. Computer experiments by Brooke et al. (1992, 1994) in a DNS of channel flow examined more carefully deposition under conditions where Brownian motion is not important (the so-called "inertial impaction" regime). These studies, as well as those by Kallio and Reeks (1989) and Sun and Lin (1986), showed that a maximum in the concentration profile occurs at or very close to the wall. Thus, turbulent diffusion would bring particles away from the wall. Brooke et al. observed that particles with very large velocities disengage from the turbulence at different locations close to the wall. They continued to describe these events as free-flights, even though their observations were quite different from what was suggested by Friedlander and Johnstone. The particles could move directly to the wall and deposit with velocities characteristic of turbulence in the buffer layer or they could get trapped in a low turbulence layer in the immediate vicinity of the wall, from which they deposit with velocities characteristic of the fluid turbulence in that region. Brooke et al. (1994), therefore, defined two mechanisms for deposition, depending on whether the rate is controlled by "free-flight" or "turbulent diffusion." This behavior has been verified in several recent studies (Chen and McLaughlin, 1995; van Haarlem et al., 1998; Narayanan et al., 2003). Mito and Hanratty

(2004) provide additional discussion of the model for free-flight provided by Brooke et al., but an established mathematical description is still not available.

The accumulation of particles near the wall has been interpreted in an Eulerian framework by arguing that particles are brought to the wall by a turbophoresis mechanism (Kallio and Reeks, 1989; Brooke et al., 1992, 1994). The classical approach outlined by Caporaloni et al. (1975) and by Reeks (1983) is that a drift velocity is created by a gradient in the particle velocity fluctuations

$$V_{\mathrm{tp}} = -\bar{\tau}_{\mathrm{p}} \frac{\partial \overline{v_2^2}}{\partial x_2}, \tag{1}$$

where $V_2 = \overline{V}_2 + v_2$ is the velocity in the x_2 direction. Young and Hanratty (1991) made laboratory measurements of the mean particle acceleration and showed that Eq. (1) can be obtained by considering the ensemble mean acceleration of the particles at a given location,

$$V_{\mathrm{tp}} = -\bar{\tau}_{\mathrm{p}} \frac{\overline{\mathrm{d}V_2}}{\mathrm{d}t}, \tag{2}$$

if an incompressibility assumption is made, whereby the influence of changes in the particle concentration is ignored. Young and Leeming (1997) presented a thorough investigation of this idea and derived a representation of $\overline{\mathrm{d}V_2/\mathrm{d}t}$ which includes compressibility effects. Cerbelli et al. (2001) used an approximate form of the equation developed by Young and Leeming and found that the spatial variation of the mean concentration needs to be taken into account when representing the mean particle acceleration.

The approach that has been taken to calculate the fully-developed concentration field, in an Eulerian framework, is to use a Boussinesq approximation to represent the turbulent mixing (Reeks, 1983, 2003; Johansen, 1991; Young and Leeming, 1997; Cerbelli et al., 2001):

$$\overline{C}\bar{\tau}_{\mathrm{p}} g_2 + \overline{C} V_{\mathrm{tp}} - \varepsilon \frac{\partial \overline{C}}{\partial x_2} = F_2(x_2). \tag{3}$$

where g_2 is the component of the acceleration of gravity in the x_2-direction, ε is a turbulent diffusivity and $F_2(x_2)$ is the net particle flux in the x_2-direction. The first term, representing gravitational settling, will be zero for the cases to be considered. Closure models are needed to specify $\varepsilon(x_2)$, $\overline{\mathrm{d}V_2/\mathrm{d}t}(x_2)$ and $\overline{v_2^2}(x_2)$.

The work described in this paper differs from previous analyses in that a system with wall sources is considered. This offers the simplification that, for a fully-developed condition, the flux, $F_2(x_2)$, is zero since the rates of injection and deposition are equal at each wall. The use of a stochastic method to represent the fluid turbulence allows calculations of sufficient duration that a fully developed condition is assured. The calculations differ from the stochastic analyses of Hutchinson et al. (1971), Reeks and Skyrme (1976), Kallio and Reeks (1989) in that a modified Langevin equation is used to represent the turbulence seen by the particles.

Two results to be presented in this paper are the calculations of the spatial variation of the mean acceleration and of the mean concentration. These allowed an evaluation of Eq. (1) and of the equation for $\overline{\mathrm{d}V_2/\mathrm{d}t}$ presented by Cerbelli et al. (2001). The mean concentration profiles are compared with calculations made with Eq. (3). The turbophoretic velocity is obtained from calculated $\overline{\mathrm{d}V_2/\mathrm{d}t}$ and Eq. (2) so that the use of a Boussinesq approximation could be directly tested.

A number of studies motivate a consideration of the accuracy of present methods for representing turbulent mixing: Hinze (1975) discusses results in free shear flows which suggest that dispersion, associated with large scale structures, can occur in the absence of a scalar gradient. Brooke et al. (1994) noted that free flights could stop before they reach the wall and that this type behavior could be a contributor to turbulent transport. Taylor (1921) showed that turbulent dispersion of fluid particles from a point source is time-dependent. By representing a hot wall as an array of thermal sources, Hanratty (1956) used Taylor's analysis to show that the spatial variation of turbulent diffusivities defined by a Boussinesq equation can reflect the time dependency of turbulent diffusion in addition to the spatial variation of the turbulence. (For example, the concentration field close to the wall is more strongly affected by sources which have been in the field for short time periods.) A detailed discussion of possible deficiencies of a Boussinesq approximation has been given by Reeks (2003), who used a PDF approach to describe dispersion of solid particles.

An important aspect of this study is the determination of deposition constants at large enough computer times that a fully developed condition is assured and over a much larger range of dimensionless time constants (1 to 10^5) than had previously been explored in a single calculation. Of particular importance to the description of deposition in annular flows are the delineation of the turbulent and the trajectory mechanisms and the verification of a relation recently proposed for the turbulent regime.

2. Computational approach

The system depicted in Fig. 1 is the idealized representation of an annular flow discussed in the introduction. The rectangular channel has a height of $2H$ and is infinitely wide. The flow is fully-developed and $Re_\tau = 590$. The solid spheres, that represent the drops, have a diameter of d_p. They are injected with a velocity of V_1^0, V_2^0 from the bottom wall at a rate per unit area of R_{Ab} and, from the top wall with a velocity V_1^0, $-V_2^0$ at a rate per unit area of R_{At}. They are removed from the field when they hit a wall. (At injection and deposition, the center of a particle is a distance of $d_p/2$ from a wall.) For a fully-developed condition

$$R_{Ab} = R_{Db} \quad \text{and} \quad R_{At} = R_{Dt}, \tag{4}$$

where R_{Db} and R_{Dt} are the deposition rates at the bottom and top walls (Binder and Hanratty, 1992). For the condition considered in this paper, $V_T = 0$ and the particle distribution is symmetric, so $R_{Ab} = R_{At}$ and $R_{Db} = R_{Dt}$.

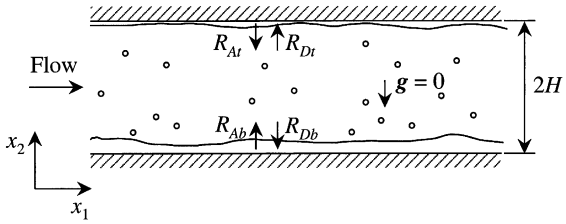

Fig. 1. Gas–liquid annular flow in a horizontal channel.

The method of analysis is described in Mito and Hanratty (2003). The two walls are considered to be the loci of instantaneous sources of particles. The contributions of these sources are summed so as to produce a fully-developed field. The theoretical problem, then, is to calculate the behavior of a single wall source. Dilute flows of particles which are much heavier than the gas are considered. Thus, lift forces (Saffman, 1965, 1968; Mei, 1992; McLaughlin, 1991; Wang et al., 1997), interparticle collisions and the influence of particles on the gas flow are ignored. These simplifying assumptions have been made in a number of previous studies (Brooke et al., 1994; van Haarlem et al., 1998; Narayanan et al., 2003). The location and velocity of a particle admitted at a time t', between 0 and t (where t is the duration of the calculation), are defined by the following equations:

$$\frac{\mathrm{d}x_i}{\mathrm{d}t} = V_i \tag{5}$$

$$\frac{\mathrm{d}V_i}{\mathrm{d}t} = -\frac{3\rho_\mathrm{f} C_\mathrm{D}}{4 d_\mathrm{p} \rho_\mathrm{p}} |\boldsymbol{V} - \boldsymbol{U}|(V_i - U_i) + g_i \tag{6}$$

where x_i is the location of the particle, V_i is the velocity of the particle, U_i is the gas velocity seen by the particle, ρ_p is the density of the particle, ρ_f is the density of the gas, and g_i, is a component of the acceleration of gravity. In the system shown in Fig. 1, x_1, x_2, x_3 are assigned to the coordinates in the streamwise, wall-normal and spanwise directions. The results presented in this paper are for the case of $g_i = 0$. The drag coefficient, C_D, is given by

$$C_\mathrm{D} = \frac{24}{Re_\mathrm{p}}(1 + 0.15 Re_\mathrm{p}^{0.687}) \tag{7}$$

where the particle Reynolds number, Re_p, is defined with d_p and the magnitude of the relative velocity $|\boldsymbol{U} - \boldsymbol{V}|$. The dimensionless inertial time constant of a particle is defined as

$$\tau_\mathrm{p}^+ = \frac{4 d_\mathrm{p}^+ (\rho_\mathrm{p}/\rho_\mathrm{f})}{3 C_\mathrm{D} |\boldsymbol{V}^+ - \boldsymbol{U}^+|}. \tag{8}$$

For a Stokes law resistance

$$\tau_\mathrm{pS}^+ = \frac{d_\mathrm{p}^{+2} (\rho_\mathrm{p}/\rho_\mathrm{f})}{18}. \tag{9}$$

In the non-Stokes region the average of τ_p^+ is a function of x_2. Thus, the volume-averaged inertial time constant τ_pB^+ is a more appropriate parameter to describe particle turbulence:

$$\tau_\mathrm{pB}^+ = \frac{1}{2HC_\mathrm{B}} \int_0^{2H} \bar{\tau}_\mathrm{p}^+(x_2)\overline{C}(x_2)\,\mathrm{d}x_2, \tag{10}$$

where C_B is a bulk concentration defined as

$$C_\mathrm{B} = \frac{1}{2H} \int_0^{2H} \overline{C}(x_2)\,\mathrm{d}x_2. \tag{11}$$

For some of the conditions considered in this paper, τ_pB^+ could be six times larger than τ_pS^+.

All of the particles admitted at a time t' eventually deposit, so that for large enough t a fully developed condition is reached for which contributions were made from sources which entered the field at a number of previous times. The time required for all of the particles from a source to deposit increases dramatically with decreasing τ_p^+. Integral time periods of $t^+(=tv^{*2}/v)=5\times10^4$ to 2×10^8 were needed to reach stationary states for τ_{pS}^+ values ranging from 1 to 40. Clearly this calculation would not be feasible for a DNS at $Re_\tau=590$. Calculations in which contributions by Brownian motion were included had durations of $t^+=1\times10^8$ for $\tau_{pS}^+=1$ and $t^+=3\times10^6$ for $\tau_{pS}^+=5$.

The fluid velocity in Eq. (6) is represented as the sum of a mean component, obtained from Eulerian measurements, and a fluctuating component, u_i. The use of a Langevin equation to represent the fluid velocity seen by particles has been explored by Perkins (1992), Sommerfeld et al. (1993), Pozorski and Minier (1998), Iliopoulos et al. (2003) and Mito and Hanratty (2003). This approach is pursued in the present paper.

In its simplest form, the Langevin equation consists of a damping force and a Wiener process which calculates velocities of passive tracers by assuming they are approximated by a Markov sequence. Lin and Reid (1963) and Obukhov (1959) applied the Langevin equation to homogeneous isotropic turbulence. The change in the velocity of a tracer over a time interval dt was given by

$$du_i=-\frac{u_i}{\tau_i}dt+d\mu_i, \tag{12}$$

where τ_i is a time constant. The forcing function $d\mu_i$ has a zero mean and is given by a Gaussian function. This equation provides the same result as obtained by Taylor (1921) in his analysis of dispersion from a point source if the Lagrangian correlation is represented by $\exp(-t/\tau_L)$ and $\tau_i=\tau_L$, the Lagrangian time scale.

The Langevin equation has been adapted to describe dispersion of fluid particles in nonhomogeneous fields by Durbin (1983, 1984), Hall (1975), Iliopoulos and Hanratty (1999), Legg and Raupach (1982), Reid (1979), Reynolds (1997), Thomson (1984, 1986, 1987), van Dop et al. (1985) and Wilson et al. (1981).

We have used the approach of Wilson et al. (1981) and of Thomson (1984), whereby

$$d\left(\frac{u_i}{\sigma_i}\right)=-\frac{u_i}{\sigma_i\tau_i}dt+\overline{d\mu_i}+d\mu_i', \tag{13}$$

where the forcing function, the time scale, τ_i, and the root-mean square of the velocity fluctuations, σ_i, are functions of x_2. The forcing function, $d\mu_i$, consists of a mean component, $\overline{d\mu_i}$, and a fluctuating component, $d\mu_i'$. The fluctuating component is assumed to be Gaussian. A number of investigators have shown that $\overline{d\mu_i}$ must be nonzero in order to avoid spatial accumulations which are not physical. The mean drift, $\overline{d\mu_i}$, and the covariance, $\overline{d\mu_i'd\mu_j'}$, are derived from Eq. (13) by neglecting terms of higher order than dt (Iliopoulos and Hanratty, 1999; Mito and Hanratty, 2002) as

$$\overline{d\mu_i}=\frac{\partial\left(\overline{u_2u_i}/\sigma_i\right)}{\partial x_2}dt, \tag{14}$$

$$\overline{\mathrm{d}\mu_i' \mathrm{d}u_j'} = \frac{\overline{u_i u_j}}{\sigma_i \sigma_j}\left(\frac{1}{\tau_i} + \frac{1}{\tau_j}\right)\mathrm{d}t, \tag{15}$$

where an overbar indicates an ensemble average. It is noted that the nonzero terms in Eqs. (14) and (15) are $\overline{\mathrm{d}\mu_1}$, $\overline{\mathrm{d}\mu_2}$, $\overline{\mathrm{d}\mu_1'^2}$, $\overline{\mathrm{d}\mu_2'^2}$, $\overline{\mathrm{d}\mu_3'^2}$, $\overline{\mathrm{d}\mu_1'\mathrm{d}\mu_2'}$, for the flow field that is considered and that jointly Gaussian random variables, $\mathrm{d}\mu_i'$, of which covariances are given by Eq. (15) are generated every time step. Mito and Hanratty (2002) showed that the Lagrangian stochastic method that is defined by Eqs. (13)–(15) for dispersion of fluid particles satisfies the condition of well-mixedness (Thomson, 1987). These equations and the numerical procedure for solving them are described in detail by Mito and Hanratty (2003). This includes approximating the Lagrangian time constants, τ_i, as characterizing the dispersion of fluid particles from sources at different x_2 (Mito and Hanratty, 2002). The values of τ_i (x_2) used in the simulation at $Re_\tau = 590$ are given by Mito and Hanratty (2004). The DNS database for turbulent channel flow at $Re_\tau = 590$, obtained by Moser et al. (1999), provided the mean velocities of the fluid and the turbulent statistics that appear in Eqs. (13)–(15). The computational time step used in Eqs. (5), (6), (13) was $\Delta t^+ = \Delta t\ v^{*2}/\nu = 0.5$.

Eq. (13) requires the time constants characterizing the fluid turbulence seen by the particles. These can be different from the time constants characterizing the dispersion of fluid particles. The basic notion in using Eq. (13) was that the τ_i for fluid particles would need to be adjusted to recognize that the dispersing particles do not follow the fluid and that the ratio of the time constant used in Eq. (13) to the time constant characterizing the dispersion of fluid particles could be a function of the inertial time constants of the particles and their free fall velocities. A preliminary study revealed that good results could be obtained by simply equating the τ_i in Eq. (13) to the time constant of the fluid particles.

For example, the broken lines in Fig. 2 are values of τ_i obtained in a DNS at $Re_\tau = 150$ for sources of fluid particles located at different locations in the channel. These were determined by calculating the time at which the Lagrangian correlation coefficient reaches a value of $R_i = 0.368$. (This choice defines τ_i as the area under the correlation curve if $R_i(t) = \exp(-t/\tau_i)$.) The points shown in Fig. 2 were obtained by calculating the temporal correlation of fluid velocity

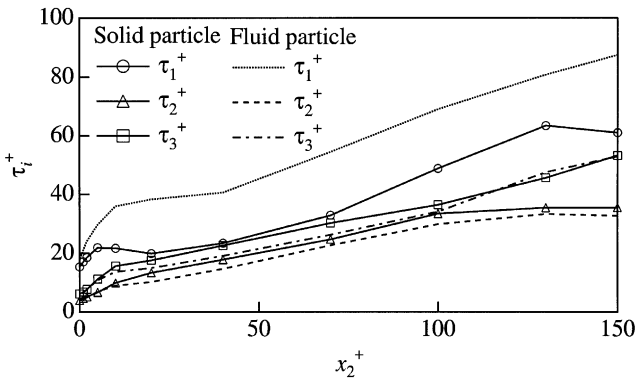

Fig. 2. Plots of Lagrangian time scales of velocity fluctuations of fluid particles and of fluid velocity fluctuations seen by solid particles of $\tau_{ps}^+ = 20$ and no gravity, measured in a DNS at $Re_\tau = 150$.

fluctuations seen by particles for the condition $\tau_{pS}^{+} = 20$ and $g_i = 0$. The τ_2^{+} and τ_3^{+} are seen to be close to the values obtained by examining the dispersion of fluid particles. The τ_1^{+} are lower. However, the calculations presented in this paper are relatively insensitive to the choice of τ_1^{+}.

3. Scope of the computations

The computations involved the introduction of $N_b(=10{,}000)$ particles from the top and bottom walls for cases in which Brownian motion was not considered. Woodmansee and Hanratty (1969) have shown that atomization of wall films occurs by a rapid growth and removal of capillary waves which create drops that are entrained by the turbulence in a region outside the viscous wall layer. This would suggest that, in the absence of more data, drops should be placed in the field at a short distance from the wall with a velocity characteristic of the mean velocity and the root-mean square of the velocity fluctuations just outside the viscous wall layer. We have chosen to use an injection velocity of $(V_1^{0+}, V_2^{0+}, V_3^{0+}) = (15, 1, 0)$ at the bottom wall and $(V_1^{0+}, V_2^{0+}, V_3^{0+}) = (15, -1, 0)$ at the top wall. The calculated deposition constants are relatively insensitive to the choice of V_i^0, except at large τ_p^{+} where the particles move in trajectories which are not affected by the fluid turbulence. The rates of atomization and deposition at the bottom and top walls are calculated as $N_b/A\Delta t$ where A is the area of the wall over which the particles are discharged and Δt is the time interval over which N_b particles are admitted from a wall source.

The concentration fields and statistics for the particle velocity fields were calculated with first-order weights for each particle. This was done by using the distances between the centers of the particles and the sampling points between which the center of the particle exists (Mito and Hanratty, 2004). The 129 points, $x_2^j (j = 1\text{–}129)$, were distributed from $x_2 = d_p/2$ to $x_2 = 2H - d_p/2$ with a cosine function, which gives bin sizes of $\Delta x_2^{+} = 0.088$ at the walls and $\Delta x_2^{+} = 14.4$ at the center of the channel for the cases of $d_p^{+} = 0.368$. Sixty-four sampling points were also distributed in the regions of $x_2^1 \leqslant x_2 \leqslant x_2^3$ and of $x_2^{127} \leqslant x_2 \leqslant x_2^{129}$ in the calculations of concentration profiles (for $\tau_{pS}^{+} \leqslant 250$) in order to capture the detailed near-wall behavior. This gives a bin size of $\Delta x_2^{+} = 1.1 \times 10^{-4}$ at a wall for the cases of $d_p^{+} = 0.368$. It is noted that the computational time step $\Delta t^{+} = 0.5$ is not small enough to resolve the contributions of the particles in the injection process that have been in the field for $t^{+} < 1$. These small bins can be used only for the determination of concentration fields for $\tau_{pS}^{+} \leqslant 250$, for which the contributions by the injection process to the concentration fields are negligibly small compared to the total concentration in the regions very close to the walls. They were not used in the calculation of particle velocity fields because the contributions of the particles involved in the injection process to the average velocity fields could not be ignored.

Distribution functions of the wall-normal velocity components of the depositing particles are calculated by using the first-order sampling method and 65 bins distributed from $V_d^{+} = 0$ to $V_d^{+} = 2$ with a hyperbolic tangent function which gives bin sizes of $\Delta V_d^{+} = 1.7 \times 10^{-5}$ at $V_d^{+} = 0$ and $V_d^{+} = 7.7 \times 10^{-2}$ at $\Delta V_d^{+} = -2$.

In the calculations in which the influence of Brownian motion was included, we used the approach adapted by Ounis et al. (1991) and by Chen and McLaughlin (1995). The dimensionless Brownian force is described as

$$F_{\mathrm{B}i}^{+} = \xi_i \sqrt{\frac{2}{Sc\tau_{\mathrm{pS}}^{+2}\Delta t^{+}}}, \tag{16}$$

where Sc is the Schmidt number and ξ_i is a Gaussian random number. The Schmidt number is defined as

$$Sc = \frac{v}{D} = \frac{3\pi v^2 \rho_{\mathrm{f}} d_{\mathrm{p}}}{C_{\mathrm{c}} kT} = \frac{3\pi v^3 \rho_{\mathrm{f}} d_{\mathrm{p}}^{+}}{C_{\mathrm{c}} kTv^{*}}, \tag{17}$$

where C_{c} is the Cunningham slip factor, k is the Boltzmann constant, T is the absolute temperature and the gas is assumed to be air at atmospheric conditions. The friction velocity, v^{*}, is assumed to be 0.6 m/s (Lee et al., 1989; Chen and McLaughlin, 1995) in order to determine $d_{\mathrm{p}} = d_{\mathrm{p}}^{+} v/v^{*}$ in Eq. (17). It is noted that the amplitude of the dimensionless Brownian force varies as $v^{*1/2}$, so that it increases with increases in v^{*}. The momentum equation of a particle is defined as

$$\frac{\mathrm{d}V_i}{\mathrm{d}t} = -\frac{3\rho_{\mathrm{f}} C_{\mathrm{D}}}{4 d_{\mathrm{p}} \rho_{\mathrm{p}} C_{\mathrm{C}}} |\boldsymbol{V} - \boldsymbol{U}|(V_i - U_i) + F_{\mathrm{B}i} + g_i, \tag{18}$$

where the Cunningham slip factor is introduced into the drag term as was done by Zhang and Ahmadi (2000). In this study, the Brownian force that is defined by Eq. (16) was used only in the calculations for $\tau_{\mathrm{pS}}^{+} = 1$, 3 and 5, for which the Stokes law is applicable. Simulations without the Brownian effect were also done for these τ_{pS}^{+}.

Two sets of calculations were carried out: In one of these, the dimensionless particle diameter was kept constant at $d_{\mathrm{p}}^{+} = 0.368$ and the particle time constant was varied by changing $\rho_{\mathrm{p}}/\rho_{\mathrm{f}}$ (See Eq. (9)). In the second, $\rho_{\mathrm{p}}/\rho_{\mathrm{f}}$ was kept constant at a value of 1000 (characteristic of gas–liquid dispersed flow at atmospheric conditions) and the particle time constant was varied by changing d_{p}^{+}.

Fig. 3 presents calculations of the bulk averaged particle Reynolds number, Re_{pB}, calculated for different τ_{pS}^{+} (defined by Eq. (9)). The Brownian force is not included in the calculations. It is noted for $d_{\mathrm{p}}^{+} = 0.368$ that $Re_{\mathrm{pB}} < 2$ so that Stokes law is a good approximation for the whole range of $\rho_{\mathrm{p}}/\rho_{\mathrm{f}}$ that was studied. Thus $\tau_{\mathrm{pS}}^{+} \cong \tau_{\mathrm{pB}}^{+}$. For $\rho_{\mathrm{p}}/\rho_{\mathrm{f}} = 1000$ the particle Reynolds number is larger than unity for a large range of conditions.

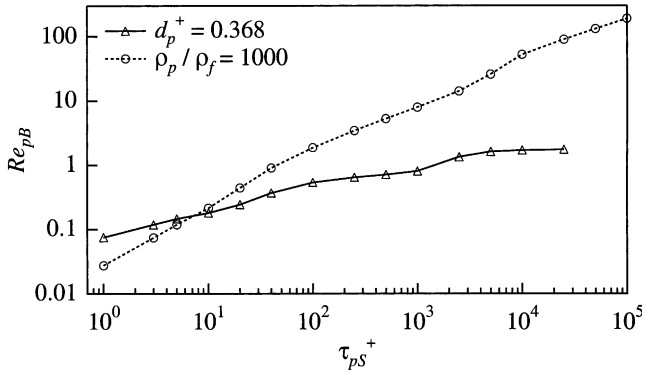

Fig. 3. Variations of particle Reynolds number against the Stokesian inertial time constant.

Table 1
Stokesian and bulk-mean particle inertial time constants and bulk-mean particle Reynolds numbers for the conditions calculated

$d_p^+ = 0.368$				$\rho_p/\rho_f = 1000$			
τ_{pS}^+	τ_{pB}^+	Re_{pB}	ρ_p/ρ_f	τ_{pS}^+	τ_{pB}^+	Re_{pB}	d_p^+
1	0.977	0.0748	1.33×10^2	1	0.988	0.0274	0.134
3	2.91	0.118	4.00×10^2	3	2.92	0.0740	0.232
5	4.82	0.147	6.65×10^2	5	4.84	0.118	0.300
10	9.55	0.181	1.33×10^3	10	9.52	0.214	0.424
20	18.9	0.242	2.65×10^3	20	18.5	0.441	0.600
40	37.2	0.367	5.30×10^3	40	35.2	0.901	0.848
100	91.4	0.536	1.33×10^4	100	81.9	1.87	1.34
250	226	0.643	3.32×10^4	250	187	3.45	2.12
500	449	0.712	6.65×10^4	500	344	5.27	3.00
1000	888	0.810	1.33×10^5	1000	624	7.93	4.24
2500	2120	1.34	3.32×10^5	2500	1310	14.2	6.70
5000	4150	1.62	6.65×10^5	5000	2120	25.8	9.48
10,000	8260	1.71	1.33×10^6	10,000	3180	52.1	13.4
25,000	20,500	1.76	3.32×10^6	25,000	6070	89.8	21.2
				50,000	9960	131	30.0
				100,000	16,200	189	42.4

A difficulty in choosing run conditions is that τ_{pB}^+ is not known a priori. Therefore, in the calculations for $\rho_p/\rho_f = 1000$ a range of τ_{pS}^+ (or d_p^+) was selected so that the same range of τ_{pB}^+ used for $d_p^+ = 0.368$ was covered. Table 1 summarizes the conditions for the calculations. It is noted that a range of $\tau_{pB}^+ = 1$–$20,000$ was covered. This required a variation of τ_{pS}^+ of 1–100,000 for the runs with $\rho_p/\rho_f = 1000$.

As can be seen in Table 1 calculations for $d_p^+ = 0.368$ requires a variation of ρ_p/ρ_f from 1.33×10^2 to 3.32×10^6. It is probably not feasible to realize the very large density ratios in the laboratory and still keep $Re_\tau = 590$. Therefore, a consideration of these results would be of interest only from the viewpoint of examining the calculations over a large range of parameter space. The calculations for $\rho_p/\rho_f = 1000$ required a consideration of large particle Reynolds numbers and large d_p^+ for which one could expect the existence of particle wakes which could influence the fluid flow field. However, it will be noted (Fig. 9) that these conditions would exist only in the range of τ_{pB}^+ where fluid turbulence is not important. Therefore, the calculations are of interest in examining the particle behavior in the trajectory regime.

4. Results

4.1. Particle turbulence

Calculations for the particle turbulence were found to be the same both for the studies with $d_p^+ = 0.368$ and the studies with $\rho_p/\rho_f = 1000$, and to be a function of τ_{pB}^+. Furthermore, no

difference could be noted when the effects of Brownian motion were included. Therefore, only results for $d_p^+ = 0.368$ are discussed in this subsection.

Fig. 4a presents root-mean-square values of the fluctuations of the wall-normal particle velocity, $(\overline{v_2^2})^{1/2}$, for $d_p^+ = 0.368$ and $\tau_{pS}^+ = 1$–250. These include contributions of motions excited by the fluid turbulence and contributions of the injected particles. In the outer flow the former of these seems to dominate for $\tau_{pS}^+ = 1$–40. The decrease of $(\overline{v_2^2})^{1/2}$, with increasing τ_p^+ has been noted by a number of investigators. (See, for example, Reeks (1977).) It arises because the inertia of the particles prohibits their following the fluid fluctuations exactly. An equation proposed by Lee et al. (1989) very roughly captures the behavior for $\tau_{pS}^+ = 1$–40:

$$\overline{v_2^2} = \left(\frac{\tau_{L2}/\overline{\tau}_p}{0.7 + \tau_{L2}/\overline{\tau}_p}\right)\overline{u_2^2}. \tag{19}$$

where τ_{L2} is the Lagrangian time scale in the x_2 direction for the fluid.

Results on the behavior of a single wall source (Mito and Hanratty, 2003) show that particles injected from the wall are transported to a distance slightly less than the stopping distance in a stationary fluid,

$$x_{2\ \mathrm{stop}}^+ \cong 0.65 V_2^{0+} \tau_{pS}^+, \tag{20}$$

where they then mix with the particles in the field. This is illustrated in Fig. 4b, which focuses on the region close to the wall. Eq. (20) is indicated by arrows for the different τ_{pS}^+ represented in the

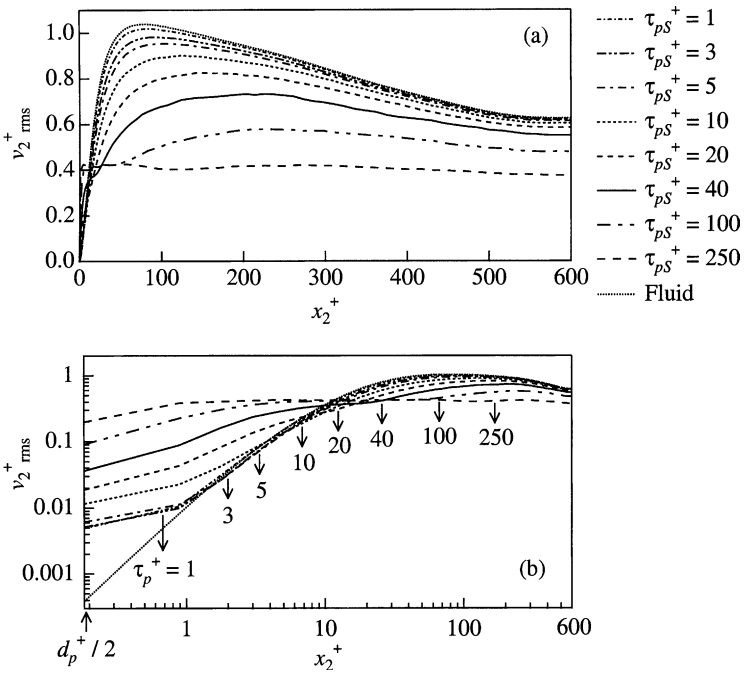

Fig. 4. Root-mean-square values of wall-normal fluctuating component of particle velocity in (a) arithmetic and (b) logarithmic coordinates ($d_p^+ = 0.368$).

figure. Deviations from the type behavior observed for the fluid turbulence close to the wall are initiated approximately at $x_{2\ \mathrm{stop}}$. It is not captured for $\tau_{\mathrm{pS}}^{+} = 1$ due to the insufficient resolution of the particle turbulence in the region in the immediate vicinity of the wall.

The concentration in the bin adjacent to the wall may be considered to consist of two populations. One with concentration $C_{\mathrm{W}+}$ contains only the injected particles and the other with concentration $C_{\mathrm{W}-}$ includes depositing particles and other particles that have stagnated close to the wall. The average value of $\overline{v_2^2}$ at the wall therefore can be represented by

$$\overline{v_2^2}|_{x_2=d_{\mathrm{p}}/2} = \frac{C_{\mathrm{W}+}(V_2^0)^2 + C_{\mathrm{W}-}(\overline{V}_{\mathrm{W}})^2}{C_{\mathrm{W}}} \tag{21}$$

where V_2^0 is the wall-normal velocity component of the injected particles and $\overline{V}_{\mathrm{W}}$ is the mean wall-normal velocity of the other particles at the wall. The rates of injection and deposition are given as the products of the concentrations and the mean velocities:

$$R_{\mathrm{Ab}} = C_{\mathrm{W}+}V_2^0, \tag{22}$$

$$R_{\mathrm{Db}} = -C_{\mathrm{W}-}\overline{V}_{\mathrm{W}}. \tag{23}$$

Since $R_{\mathrm{Ab}} = R_{\mathrm{Db}}$ in the fully-developed field and $C_{\mathrm{W}} = C_{\mathrm{W}+} + C_{\mathrm{W}-}$, the quantities $C_{\mathrm{W}+}$ and $C_{\mathrm{W}-}$ can be eliminated from Eq. (21) to give

$$\overline{v_2^2}|_{x_2=d_{\mathrm{p}}/2} = -V_2^0\overline{V}_{\mathrm{W}}. \tag{24}$$

Thus, since $V_2^{0+} = 1$, the values of $(\overline{v_2^2})^{1/2}$ shown in Fig. 4b at $d_{\mathrm{p}}^{+}/2$ equal $(-\overline{V}_{\mathrm{W}})^{1/2}$. The increase of $-\overline{V}_{\mathrm{W}}$ with increasing τ_{pS}^{+} results from the increased importance of deposition by free-flight. Because of the contribution of the injected particles, indicated by Eq. (24), $(\overline{v_2^2})^{1/2}$ also assumes larger values than the fluid velocity fluctuations for $\tau_{\mathrm{pS}}^{+} = 1$, 3 and 5, at which free-flight is not the main contributor to the particle flux to wall.

For $\tau_{\mathrm{pS}}^{+} = 100$ and 250 it is seen in Fig. 4b that the influence of injection velocity extends over a much larger x_2^{+}. Results presented in Fig. 5 for $\tau_{\mathrm{pS}}^{+} > 250$ are seen to be strongly influenced by the injection velocity over the whole channel cross section. For a given τ_{pS}^{+}, the $\overline{v_2^2}$ are roughly independent of x_2^{+}. For $\tau_{\mathrm{pS}}^{+} > 1000$ the root-mean square of v_2 increases with increasing τ_{pS}^{+}. A limiting

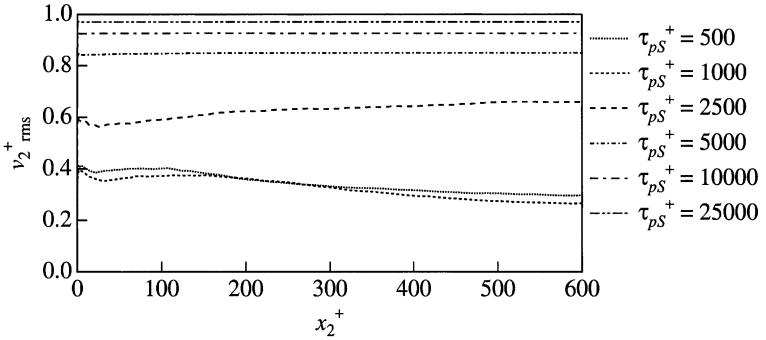

Fig. 5. Root-mean-square values of wall-normal fluctuating component of particle velocity for $\tau_{\mathrm{pS}}^{+} \geqslant 500 (d_{\mathrm{p}}^{+} = 0.368)$.

value of $(\overline{v_2^2})^{1/2}$ is suggested at very large τ_p^+ for which injected particles proceed from one wall to the other in a unidirectional trajectory without slowing down. This limiting value equals 1 since particles are injected at a velocity of $V_2^{0+} = 1$. The calculations for $\tau_{pS}^+ = 5000$, 10,000, 25,000 indicate a behavior which is very close to this.

4.2. Mean particle accelerations

Mean values of the particle acceleration for $d_p^+ = 0.368$ are used to evaluate the turbophoretic velocities defined by Eq. (2). In the system used in this study, the turbophoretic velocity is exactly defined from Eq. (6) as

$$V_{tp} = -\overline{\tau_p \frac{dV_2}{dt}}, \tag{25}$$

where τ_p^+ is the local value obtained from Eq. (8). Turbophoretic velocities defined by Eq. (25) are plotted in Fig. 6. In the system considered, Eq. (2) was found to give almost the same results as Eq. (25). At the center of the channel V_{tp}^+ is zero because of symmetry. It is also observed to be zero at $x_2^+ \cong 80$ for $\tau_{pS}^+ \leqslant 100$. In the outer region the turbophoretic velocities have positive values, that is, away from the wall. In the wall region, the particles have mean convective velocities toward the wall.

The magnitude of the turbophoretic velocity is seen to increase with increasing τ_{pS}^+, even though the magnitude of $\overline{dV_2^+/dt^+}$ is decreasing. The slowing of the injected particles as they move out into the fluid provides negative contributions to dV_2^+/dt^+ or positive contributions to V_{tp}^+. For $\tau_{pS}^+ \leqslant 20$ this effect is not evident. However, the deceleration of the injected particles probably accounts for the decrease in the magnitude of V_{tp}^+ at $x_2^+ \cong 20$ with the increase of τ_{pS}^+ from 20 to 40.

The variation of V_{tp} is in qualitative agreement with classical relation given by Eq. (1). However, as illustrated in Fig. 7 for $\tau_{pS}^+ = 5$, it overpredicts the magnitude for $x_2^{+*} < 200$. Young and Leeming (1997) started with the following relation in an Eulerian framework for the mean acceleration of solid particles in a fully-developed field:

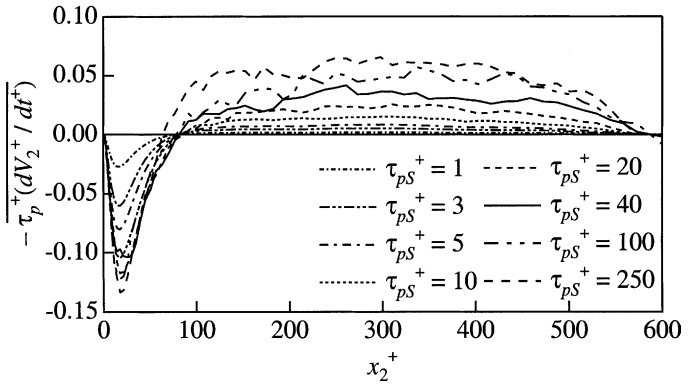

Fig. 6. Turbophoretic velocities ($d_p^+ = 0.368$).

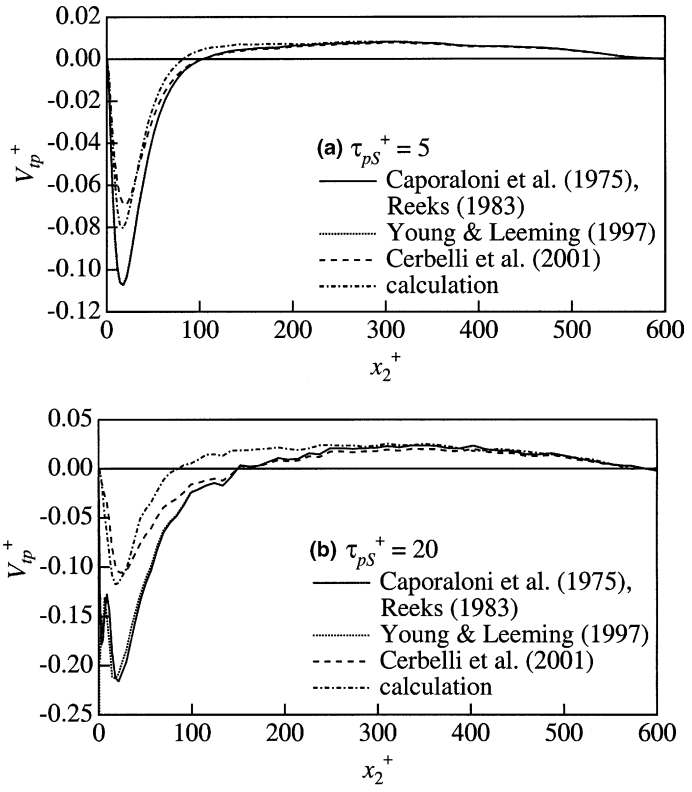

Fig. 7. Test of theories of turbophoretic velocity ($d_p^+ = 0.368$). (a) $\tau_{pS}^+ = 5$, (b) $\tau_{pS}^+ = 20$.

$$\overline{\frac{dV_2}{dt}} = \overline{V}_2 \frac{\partial \overline{V}_2}{\partial x_2} + \frac{\partial \overline{v_2^2}}{\partial x_2} - \overline{v_2 \frac{\partial v_i}{\partial x_i}}, \tag{26}$$

From conservation mass considerations,

$$\frac{\partial v_i}{\partial x_i} = -\frac{\partial(\ln C)}{\partial t} - V_i \frac{\partial(\ln C)}{\partial x_i} - \frac{\partial \overline{V}_i}{\partial x_i}. \tag{27}$$

They substituted Eq. (27) into Eq. (26) and assumed that $\partial(\ln C)/\partial t$ is not correlated with v_2 to obtain

$$\overline{\frac{dV_2}{dt}} = \overline{V}_2 \frac{\partial \overline{V}_2}{\partial x_2} + \frac{\partial \overline{v_2^2}}{\partial x_2} + \overline{v_2 V_i \frac{\partial(\ln C)}{\partial x_i}}. \tag{28}$$

In their calculations they ignored the last term in Eq. (28) and, therefore, represented the mean acceleration as

$$\overline{\frac{dV_2}{dt}} \cong \overline{V}_2 \frac{\partial \overline{V}_2}{\partial x_2} + \frac{\partial \overline{v_2^2}}{\partial x_2}. \tag{29}$$

As shown in Fig. 7, Eq. (29) does not produce predictions (for the cases considered in this paper) that are much different from Eq. (1). Cerbelli et al. (2001) included effects of spatial variations of C by using Eq. (28) with the following approximation

$$\overline{v_2 V_i \frac{\partial(\ln C)}{\partial x_i}} \cong \overline{v_2^2} \frac{\partial(\ln \overline{C})}{\partial x_2}. \tag{30}$$

The prediction of Cerbelli et al. roughly agrees with the calculations using Eq. (25).

4.3. Rates of deposition for $d_p^+ = 0.368$

Cumulative fractions of the flux of particles, depositing with velocities of $V_d^+ < V_2^+ < 0$, are presented in Fig. 8 for the case of $d_p^+ = 0.368$. For $\tau_{pS}^+ = 1$, 3, 5 particles are mainly depositing with very small velocities, $10^{-4} < -V_d^+ < 10^{-3}$. These are of the order of the wall-normal fluid velocity fluctuations at $d_p^+/2$. For this range of variables, particles trapped close to the wall appear to be depositing by "turbulent diffusion" (Mito and Hanratty, 2004). For $\tau_{pS}^+ = 10$, 20, 40, 100, 250, the particles are depositing, mainly, with velocities which are characteristic of fluid velocity fluctuations in the region outside the viscous sublayer. Particles with these velocities are pictured to move in "free-flight" through the layer of trapped particles close to the wall.

Plots of the mean deposition velocity are presented in Fig. 9a. A strong variation with τ_{pB}^+ is not noted in the "turbulent diffusion" regime, $\tau_{pB}^+ = 1$–5, since the $-\overline{V}_d^+$ largely result from the fluid velocity fluctuations at $d_p/2$. The slight increase with decreasing τ_{pB}^+ could reflect the improved ability of the particles to follow the fluid turbulence. The increase in $-\overline{V}_d^+$ in the region $5 < \tau_B^+ < 250$ occurs because, on average, free-flight to the wall is initiated at larger distances from the wall as τ_{pB}^+ increases.

This consideration plus the recognition that the concentration profiles become more uniform with increasing τ_p^+ lead Hay et al. (1996), Hanratty et al. (2000), Pan and Hanratty (2002b) to suggest that deposition in annular flow is dominated by particles that start their free-flight outside the viscous wall layer so that

$$k_D = \frac{\sigma_p}{\sqrt{2\pi}}, \tag{31}$$

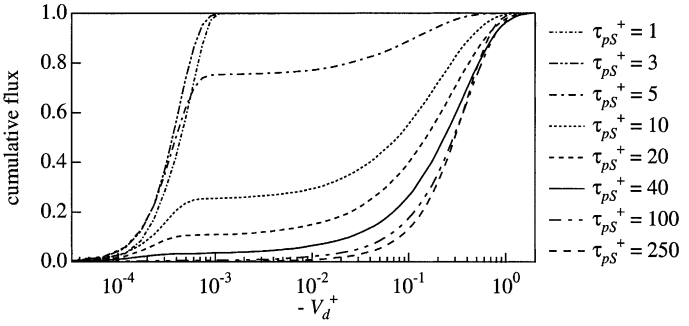

Fig. 8. Cumulative fraction of contribution of particles with velocities $\geqslant V_{d^+}$ to the total deposition flux ($d_p^+ = 0.368$).

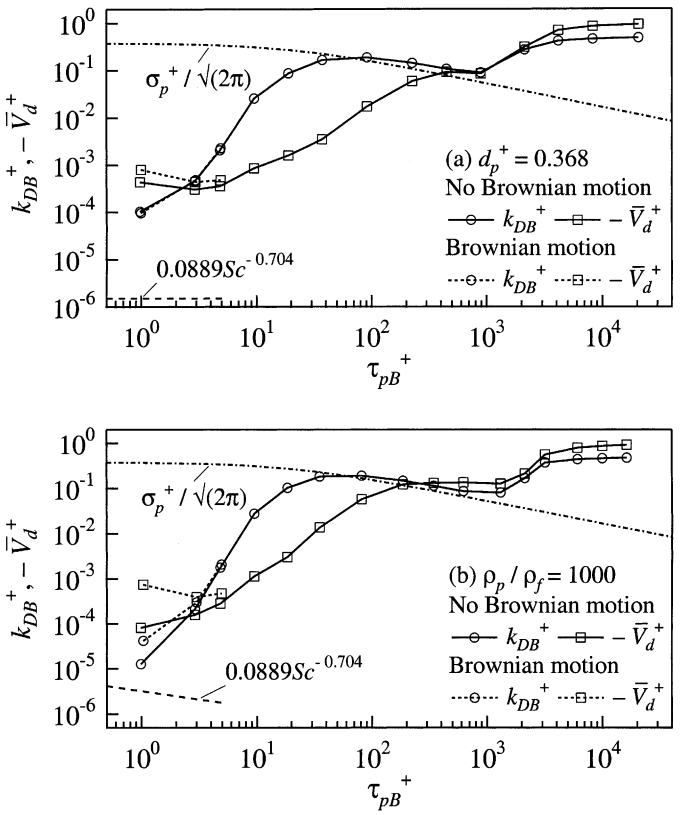

Fig. 9. Deposition constants defined with the bulk-mean concentration, k_{DB}^{+}, and average velocities of depositing particles, $-\overline{V}_{\mathrm{d}}^{+}$, for the cases of (a) $d_p^{+} = 0.368$ and (b) $\rho_{\mathrm{p}}/\rho_{\mathrm{f}} = 1000$.

where σ_{p} is the root-mean-square of the wall-normal velocity fluctuations of the particles and a Gaussian distribution is assumed. This equation is plotted with dots and dashes in Fig. 9a. The σ_{p} were calculated at $x_2^{+} = 40$ by using Eq. (19) to relate the particle turbulence to the fluid turbulence. It is noted in Fig. 9a that $-\overline{V}_{\mathrm{d}}^{+}$ reaches a value approximately equal to Eq. (31) at $\tau_{\mathrm{pB}}^{+} = 400$. It is also noted from Eq. (20) that $x_{2\mathrm{stop}}^{+} \cong 2H^{+}$ at $\tau_{\mathrm{pS}}^{+} = 1800$, since $V_2^{0+} = 1$. This suggests that particles could be depositing by free-flight unidirectional trajectories that start from the opposite wall. At extremely large τ_{pS}^{+} these would arrive at roughly the same velocity at which they are injected. The observation of $-\overline{V}_{\mathrm{d}}^{+} \cong 1$ at $\tau_{\mathrm{pB}}^{+} \cong 5000$ is consistent with this interpretation.

A deposition constant defined as

$$k_{\mathrm{DB}}^{+} = \frac{R_{\mathrm{Ab}} + R_{\mathrm{At}}}{2C_{\mathrm{B}}v^{*}} = \frac{R_{\mathrm{Ab}}}{C_{\mathrm{B}}v^{*}}, \tag{32}$$

is also plotted in Fig. 9a. By considering Eqs. (22) and (23)

$$\overline{C}_{\mathrm{W}}^{+} = \frac{\overline{C}_{\mathrm{W}}v^{*}}{R_{\mathrm{Ab}}} = \frac{1}{V_2^{0+}} - \frac{1}{\overline{V}_{\mathrm{W}}^{+}}. \tag{33}$$

Thus, when $|\overline{V}_W^+| \ll V_2^{0+}$, $\overline{C}_W^+ = -1/\overline{V}_W^+$; that is, the injected particles are not influencing the concentration at the wall. This holds for $\tau_{pB}^+ < 1000$. Then, if the sampling volume at the wall is small enough $\overline{V}_W^+ = \overline{V}_d^+$ so that $-\overline{V}_d\overline{C}_W$ is equal to $R_{Db} = R_{Ab}$. From Eq. (32), it follows that changes in k_{DB}^+ represent changes in $\overline{V}_d^+$ and changes in the ratio $C_B/\overline{C}_W$, which depends on turbulent mixing away from the wall.

In classical transport processes turbulent mixing creates a concentration boundary layer in which the concentration monotonically increases, $C_B/\overline{C}_W \gg 1$ and the rate of transfer is controlled by the concentration gradient at the wall. This is realized only when Brownian motion is controlling. The increase in k_{DB}^+ with decreasing τ_{pB}^+ observed at very small $\tau_{pB}^+(\tau_{pB}^+ < 3)$ represents a transitional region in which deposition changes from a free-flight regime to a turbulent diffusion regime.

The striking feature of Fig. 9a is the sharp increase in k_{DB}^+ with increasing τ_{pB}^+ for $3 < \tau_{pB}^+ < 40$, where $-\overline{V}_d^+$ is increasing and $C_B/\overline{C}_W$ is decreasing. (See Fig. 11a.) Thus, k_{DB}^+ in this transition region depends both on the deposition velocity and on the mixing processes which govern the changes of $\overline{C}$ with x_2. For $\tau_{pB}^+ > 40$ changes in C_B with increasing τ_{pB}^+ are small (See Fig. 11a.), so changes in k_{DB}^+ reflect changes in $\overline{V}_d^+$ (or changes in the particle turbulence outside viscous wall layer).

For $100 \leqslant \tau_{pB}^+ \leqslant 1000$, the deposition constant is roughly given by Eq. (31), which has been proposed for annular flows. For $\tau_{pB}^+ > 1000$ the concentration profile is uniform and k_{DB}^+ is controlled by a trajectory mechanism. At very large τ_{pB}^+, say $\tau_{pB}^+ = 5000$, $k_{DB}^+ = -0.5\overline{V}_d^+$. For these τ_{pB}^+ the velocity of the injected particles, V_2^{0+}, equals the velocity of the depositing particles that started a trajectory from the opposite wall. Thus half of the particles at the wall are depositing, so that $\overline{V}_W^+ = -V_2^{0+}$ and $k_{DB}^+ = -0.5\overline{V}_d^+$.

As shown in Fig. 9a, Brownian motion is having a very small effect on the rate of deposition. The line on the bottom of the figure is calculated with the following equation (proposed by Shaw and Hanratty (1977) and verified by Na et al. (1999))

$$\frac{k_D}{v^*} = 0.0889Sc^{-0.704}, \tag{34}$$

for Schmidt number $= 6.0 \times 10^6$. For air at atmospheric conditions this corresponds to a friction velocity of 0.6 m/s. From Eq. (17), it is noted that k_D/v^* given by Eq. (34) varies as $v^{*0.704}$, so increases in v^* are accompanied by increases in k_D/v^*.

Fig. 9a demonstrates that annular flow can be represented by two regions in which deposition is by turbulence or by a trajectory mechanism. The latter was first proposed by Anderson and Russell (1970) and has been discussed in papers by Chang (1973), James et al. (1980) and Andreussi and Azzopardi (1983). It should be pointed out that the value of τ_{pB}^+ at which a trajectory mechanism is initiated would decrease with decreasing Re_τ and with increasing V_2^{0+}.

4.4. Rates of deposition for $\rho_p/\rho_f = 1000$

The calculations for $d_p^+ = 0.368$ used $\rho_p/\rho_f = 133$ to 3.32×10^6 in order to cover a range of τ_{pB}^+ of 1–20,000. (See Eq. (9).) Fig. 9b presents results of a more realistic calculation that keeps ρ_p/ρ_f at a constant value of 1000 (which corresponds to liquid drops in air). In this case, values of d_p^+ from 0.134 to 42.4 are needed in order to cover a range of τ_{pB}^+ of 1 to 20,000. The very small values of d_p^+

corresponding to small τ_{pS}^+ require that Brownian forces need to be considered for $\tau_{pS}^+ = 1, 3, 5$. The curve on the bottom of the figure is obtained from Eq. (34) for a friction velocity of 0.6 m/s (Chen and McLaughlin, 1995). Since d_p^+ is decreasing with decreasing τ_{pS}^+ this corresponds to a Sc variation of 1.6×10^6 to 5.0×10^6.

The calculations suggest that Brownian motion starts to control deposition some where between τ_{pB}^+ of 0.1 and 1 ($d_p = 1$–3 μm for water drops in air under atmospheric conditions). The influence of Brownian forces at small τ_{pB}^+ is manifested in several ways. If these forces are not taken into account the $-\overline{V}_d^+$ differs from what is found for the calculations with $d_p^+ =$ constant in that they continue to decrease with τ_{pB}^+ at very small τ_{pB}^+ since particles with decreasing d_p^+ see smaller fluid turbulence. However, the decrease in d_p^+ gives rise to increasing Brownian forces and therefore increasing contributions of Brownian motion to the deposition velocity. Thus $-\overline{V}_d^+$ is actually seen to increase with decreasing τ_{pB}^+.

It is interesting to note that, for $\tau_{pB}^+ > 3$, the curves representing k_{DB}^+ are roughly the same in Fig. 9a and b. This suggests the influences of d_p^+ and ρ_p/ρ_f are taken into account through a consideration of τ_{pB}^+.

Chen and McLaughlin (1995) have recently carried out a study of particle deposition in a DNS of turbulent flow in a vertical channel at $Re_\tau = 125$. The particle system was inherently nonstationary in that no sources were used for $t^+ > 0$, so that the concentration would be zero at very large times. A density ratio of $\rho_p/\rho_f = 946$ was used and inertial time constants of 0.1–50 were explored. The influences of Brownian forces and lift were included in the calculations. A deposition constant was defined by using an average concentration over the central region of the channel. We found that this average is very close to the bulk concentration used in this study.

A comparison of the k_{DB}^+ obtained by Chen and McLaughlin at $t^+ = 0$–4000 for $\tau_p{}^+ \leqslant 3$ and at $t^+ = 0$–1000 for $\tau_p^+ > 3$ with those obtained in this study for $\rho_p/\rho_f = 1000$ at very large $t^+ (t^+ \leqslant 2 \times 10^8$ for $\tau_p^+ \geqslant 1)$ is given in Fig. 10. The agreement is satisfying, considering the difference in the systems used in the two studies. It is noted that our calculations are consistent

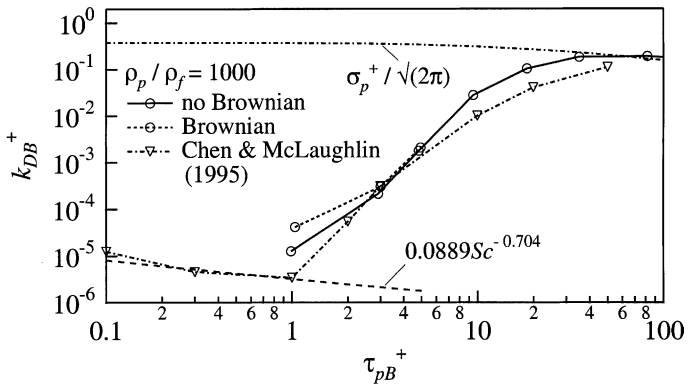

Fig. 10. Comparison of the deposition constants between the DNS results by Chen and McLaughlin (1995) and our calculation.

with the suggestion of McCoy and Hanratty (1977) that Eq. (34) is applicable to the region $\tau_{pB}^{+} \leqslant$ ca 0.3.

4.5. Concentration profiles

Concentration profiles are presented in Figs. 11 and 12 for $d_p^{+} = 0.368$ and for $\rho_p/\rho_f = 1000$. A range of $\tau_{pS}^{+} = 1$–250 is covered. (For $\tau_{pS}^{+} > 250$ a uniform concentration profile was calculated.) The injection process causes small bumps at 13, 26 and 65 for $\tau_{pS}^{+} = 20$, 40, 100. No evidence of this influence is seen for $\tau_{pS}^{+} \leqslant 10$.

A strong effect of Brownian motion is seen only in the calculation for $\tau_{pS}^{+} = 1$ and $\rho_p/\rho_f = 1000$, at which $d_p = 3$ μm. (See Fig. 12.) The shape of this profile is similar to the one calculated for $\tau_{pS}^{+} = 1$ without including the effects of Brownian forces. The chief difference is in the concentration at the wall.

It is noted in Figs. 11 and 12 that the main changes in concentration occur for $x_2^{+} < 10$. This is consistent with the suggestion that the turbophoretic drift toward the wall is playing an important role. (See Fig. 6.) Very thin concentration boundary layers with maxima at $x_2^{+} < 1$ are seen in the immediate vicinity of the wall. In this boundary layer, turbophoresis is nearly zero so turbulent diffusion is the dominant mechanism of particle transport.

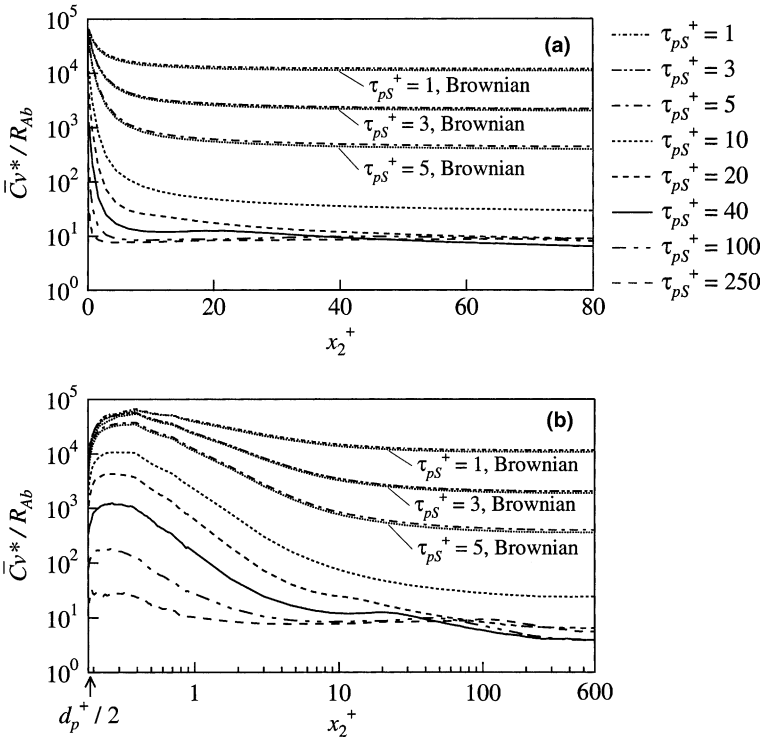

Fig. 11. Concentration fields plotted against (a) arithmetic and (b) logarithmic abscissae ($d_p^{+} = 0.368$).

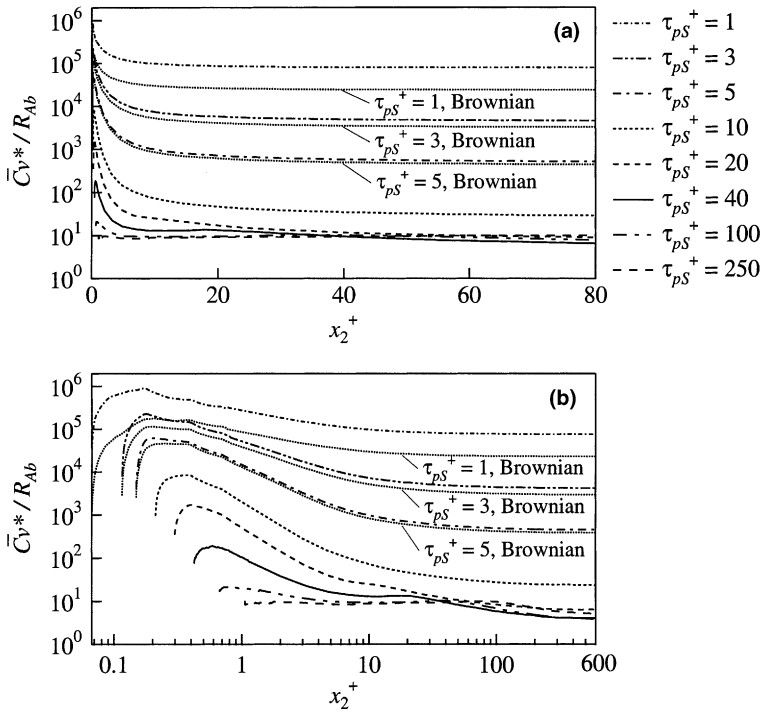

Fig. 12. Concentration fields plotted against (a) arithmetic and (b) logarithmic abscissae ($\rho_p/\rho_f = 1000$).

5. Testing of diffusion theory

Eq. (3) with $g_2 = 0$ and $F_2(x_2) = 0$ and the calculations of V_{tp} presented in Fig. 6 were used to calculate the profiles of turbulent diffusivity for $\tau_{pS}^+ = 1$, 3, 5, 10 shown in Fig. 13. A similarity in the shapes of these curves is noted. The solid curve is the diffusivity for fluid particles. The solid particle diffusivities are qualitatively and quantitatively different from the fluid diffusivities. For

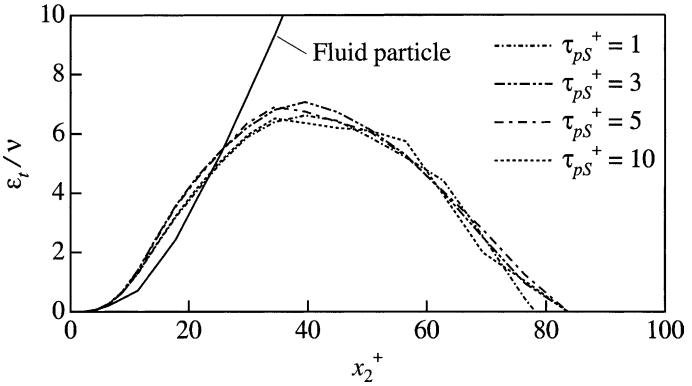

Fig. 13. Turbulent diffusivities ($d_p^+ = 0.368$).

$x_2^+ > 80$ where V_{tp}^+ takes on positive values one obtains the nonphysical result that the particle diffusivity is negative. This comparison suggests that large scale mixing that is not related to concentration gradients must be occurring.

We have chosen to discuss these differences by modifying the diffusion equation so as to include sources and sinks. These might be thought of as being due to free-flights of large velocity particles which disengage from the fluid turbulence. The diffusion equation is thus modified to be

$$\frac{\partial}{\partial x_2} V_{tp} \overline{C} + \frac{\partial}{\partial x_2}\left[-(\varepsilon + D)\frac{\partial \overline{C}}{\partial x_2}\right] = S, \tag{35}$$

where a positive value of S indicates a source and a negative value indicates a sink. (For example, locations where particles disengage from the turbulence could be considered to be sinks and locations where particles are reengaging with the turbulence could be considered as sources.) Values of S calculated for $\tau_{pS}^+ = 1, 3, 5, 10$ in this way are shown in Fig. 14 for $d_p^+ = 0.368$. In the near wall region (central column) locations between $x_2^+ = 3$ and $x_2^+ = 13$ are, on average, acting as sinks. Locations between the wall and $x_2^+ = 3$ are, on average, acting as sources. Thus, this could suggest

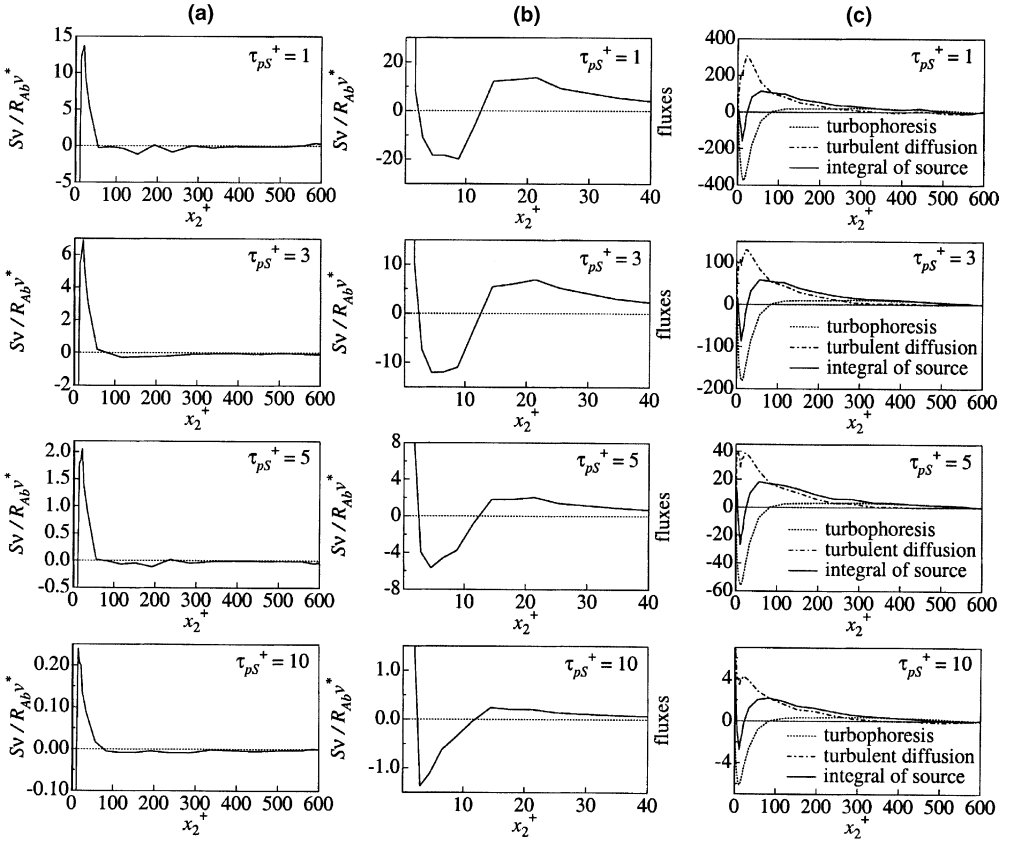

Fig. 14. Sources and sinks in the diffusion model (a) in the half-height of the channel and (b) in the near-wall region, and (c) mass flux balance ($d_p^+ = 0.368$).

that large scale transport, in addition to turbophoresis, is bringing particles to the trapped layer in the immediate vicinity of the wall. Sources exist in the region $13 < x_2^+ < 80$ and very small sinks, in the region $80 < x_2^+ < 590$. This could suggest the existence of large scale motions that transport particles from $x_2^+ > 80$ to $x_2^+ < 80$ to counterbalance the positive turbophoretic fluxes observed for $x_2^+ > 80$. Very large sources are observed adjacent to the wall. This suggests that many particles are carried into this region from outer flow by free-flights and are trapped.

Fig. 14 also presents flux balances that are obtained by integrating Eq. (35):

$$V_{\mathrm{tp}}\overline{C} - \varepsilon\frac{\partial\overline{C}}{\partial x_2} = \int_{d_\mathrm{p}/2}^{x_2} S\,\mathrm{d}y + I_0, \tag{36}$$

where $V_{\mathrm{tp}}\overline{C}$, $-\varepsilon(\partial\overline{C}/\partial x_2)$ and $\int_{d_\mathrm{p}/2}^{x_2} S\,\mathrm{d}y + I_0$, respectively, represent the mass fluxes due to turbophoresis, turbulent diffusion and sources. The term I_0 is the integration constant defined as the value of the left-hand side of Eq. (36) at $x_2^+ = d_\mathrm{p}^+/2$:

$$I_0 = \left(V_{\mathrm{tp}}\overline{C} - \varepsilon\frac{\partial\overline{C}}{\partial x_2}\right)_{x_2 = d_\mathrm{p}/2}. \tag{37}$$

The turbophoretic flux is zero at $x_2^+ = d_\mathrm{p}^+/2$ because $V_{\mathrm{tp}}^+ = 0$. Thus, the sources and sinks counterbalance the turbulent diffusion flux in the region next to the wall. This is not seen in Fig. 14c because large changes of these fluxes occur at $x_2^+ < 1$. It is noted that the particle transport by sources and sinks is not small compared to particle transport by turbophoresis and turbulent diffusion.

6. Contributions and limitations

Calculations were made for the turbulent flow, in a channel, of a suspension of spheres for which $\rho_\mathrm{p}/\rho_\mathrm{f}$ is a large number. The main contribution is the presentation of results for the concentration field and the deposition process for a larger range of inertial time constants than had previously been explored. (The effect of d_p^+ and the density ratio are found not to have a direct effect, except for very small τ_p^+.) The outcome is to provide new insights about the controlling mechanisms. Depending on the value of τ_p^+ four regimes can be defined whereby deposition is controlled by Brownian diffusion, turbulent diffusion, turbulent free-flight or unidirectional trajectories that are not affected by fluid turbulence.

Deposition in annular flows has been described as due to turbulent free-flight and, less frequently, as due to trajectories which strongly depend on the velocity with which the drops are injected into the flow from the wall film. The calculations clearly show the transition from a turbulent mechanism to a trajectory mechanism as τ_p^+ increases. These results could be of interest when considering gas–liquid flows in conduits of small dimensions. Furthermore, support is provided for an equation that has been suggested to describe turbulent deposition and a simple mathematical description of the trajectory mechanism is partially confirmed.

Of particular interest from the viewpoint of developing a theoretical description of concentration profiles is the finding that turbulent dispersion cannot be described with a Boussinesq

approximation. An evaluation of this approach is straightforward in this study since the flux under fully-developed conditions is zero, computer times (as high as $t^+ = 2 \times 10^8$) were large enough to reach a stationary state and turbophoretic velocities were determined directly. The only unknown term in the mass balance equation is the one representing Reynolds transport. Thus, turbulent diffusivities could be obtained directly from the concentration profiles. These assume unrealistic values.

We suggest that this indicates that large scale mixing, which cannot be captured by local concentration gradients, is occurring. We introduce the notion of local sources and sinks of particles in order to quantify this interpretation. This is not done in the context of suggesting a new computational approach. In fact, the discrepancies might be more fundamental in that the physics are better captured by using a Lagrangian approach.

The calculations have a number of limitations. The gravitational constant is assumed to be zero, the particle concentration is assumed to be small enough that particle–particle interactions and the influence of the particles on the fluid turbulence can be ignored. The assumption of zero gravity means that the results are best applied to vertical flows or to horizontal flows for which free fall velocity of particles is smaller than the velocity characterizing mean turbulent impaction, which is, for example, $1.4 \times 10^{-4} v^*$ for $d_p^+ = 0.368$. (See Mito and Hanratty, 2004.)

Calculations provided dimensionless concentrations, given as $C^+ = Cv^*/R_{Ab}$, so local volume fractions can be calculated if the rate of atomization is known. The suspensions that exist in annular flows typically have mean particle volume fractions of $\alpha \cong 10^{-3}$ and mean mass loadings of $\eta \cong 1$ (Hay et al., 1996; Pan and Hanratty, 2002a), so the assumption of a dilute suspension seems reasonable for this flow pattern. Nevertheless, it would be useful to carry out calculations to examine the effects of volume fraction and of mass loading. The limitation could be more serious than would be indicated by mean volume fraction since, as discussed in this paper, concentrations that are much larger than the bulk concentration can exist close to the wall. Furthermore, Yamamoto et al. (2001) and Sommerfeld (2003) examined the effects of inter-particle collisions on particle turbulence in a vertical or horizontal channel for $\eta \cong 1$ and found a noticeable redistribution of energy caused by inter-particle collisions, that is, decreases of the streamwise fluctuations and increases of the wall-normal fluctuations. Thus the results should be an accurate representation of annular flows in the low concentration region where R_D varies linearly with concentration (Hay et al., 1996; Pan and Hanratty, 2002a).

The idealized model of annular flow used in this analysis offers the advantage that a fully-developed suspension can be realized. However, the application to real annular flows is handicapped because the method for introducing drops into the flow by the atomization of the wall films is not sufficiently understood. More research in this area is needed.

Acknowledgment

This work is supported by the DOE under grant DEFG02-86ER 13556. Computer resources have been provided by the National Center for Supercomputing Applications located at the University of Illinois.

References

Anderson, R.J., Russell, T.W.F., 1970. Circumferential variation of interchange in horizontal annular two-phase flow. Ind. Eng. Chem. Fundam. 9, 340–344.

Andreussi, P., Azzopardi, B.J., 1983. Droplet deposition and interchange in annular two-phase flow. Int. J. Multiphase Flow 9, 681–695.

Binder, J.L., Hanratty, T.J., 1992. Use of Lagrangian statistics to describe drop deposition and distribution in horizontal gas liquid annular flows. Int. J. Multiphase Flow 18, 803–820.

Brooke, J.W., Kontomaris, K., Hanratty, T.J., McLaughlin, J.B., 1992. Turbulent deposition and trapping of aerosols at a wall. Phys. Fluids A 4, 825–834.

Brooke, J.W., Hanratty, T.J., McLaughlin, J.B., 1994. Free-flight mixing and deposition of aerosols. Phys. Fluids 6, 3404–3415.

Caporaloni, M., Tampieri, R., Trombetti, F., Vittori, O., 1975. Transfer of particles in nonisotropic air turbulence. J. Atmos. Sci. 32, 565–568.

Cerbelli, S., Giusti, A., Soldati, A., 2001. ADE approach to predicting dispersion of heavy particles in wall-bounded turbulence. Int. J. Multiphase Flow 27, 1861–1879.

Chang, D.R., 1973. The generation, movement and deposition of droplets in annular two-phase flow. Ph.D. Thesis, University of Delaware.

Chen, M., McLaughlin, J.B., 1995. A new correlation for the aerosol deposition rate in vertical ducts. J. Colloid Interface Sci. 169, 437–455.

Durbin, P.A., 1983. Stochastic differential equations and turbulent dispersion. NASA Reference Publication 1103.

Durbin, P.A., 1984. Comment on papers by Wilson et al. (1981) and Legg and Raupach (1982). Boundary Layer Meteorol. 29, 409–411.

Friedlander, S.K., Johnstone, H.F., 1957. Deposition of suspended particles from turbulent gas streams. Ind. Eng. Chem. 49, 1151–1156.

Hall, C.D., 1975. The simulation of particle motion in the atmosphere by a numerical random walk model. QJR Met. Soc. 101, 235–244.

Hanratty, T.J., 1956. Heat transfer through a homogeneous isotropic turbulent field. AIChE J. 2, 42–45.

Hanratty, T.J., Woods, B.D., Iliopoulos, I., Pan, L., 2000. The roles of interfacial stability and particle dynamics in multiphase flows: a personal viewpoint. Int. J. Multiphase Flow 26, 169–190.

Hay, K.J., Liu, Z.C., Hanratty, T.J., 1996. Relation of deposition to drop size when the rate law is nonlinear. Int. J. Multiphase Flow 22, 829–848.

Hinze, J.O., 1975. Turbulence, second ed. McGraw-Hill, p. 579.

Hutchinson, P., Hewitt, G.F., Dukler, A.E., 1971. Deposition of liquid or solid dispersions from turbulent gas streams: a stochastic model. Chem. Engng. Sci. 26, 419–439.

Iliopoulos, I., Hanratty, T.J., 1999. Turbulent dispersion in a non-homogeneous field. J. Fluid Mech. 392, 45–71.

Iliopoulos, I., Mito, Y., Hanratty, T.J., 2003. A stochastic model for solid particle dispersion in a nonhomogeneous turbulent field. Int. J. Multiphase Flow 29, 375–394.

James, P.W., Hewitt, G.F., Whalley, P.B., 1980. Droplet motion in two-phase flow. UKAEA Report AERE-R 9711.

Johansen, S., 1991. The deposition of particles on vertical walls. Int. J. Multiphase Flow 17, 355–376.

Kallio, G.A., Reeks, M.W., 1989. A numerical simulation of particle deposition in turbulent boundary layers. Int. J. Multiphase Flow 15, 433–446.

Lee, M.M., Hanratty, T.J., Adrian, R.J., 1989. The interpretation of droplet deposition measurements with a diffusion model. Int. J. Multiphase Flow 15, 459–469.

Legg, B.J., Raupach, M.R., 1982. Markov-chain simulation of particle dispersion in inhomogeneous flows: The mean drift velocity induced by a gradient in Eulerian velocity variance. Bounrary Layer Met. 24, 3–13.

Lin, C.C., Reid, W.H., 1963. Turbulent flow, theoretical aspects. In: Encyclopedia of Physics, Vol. 8/2. Springer-Verlag, Berlin, pp. 438–523.

McCoy, D.D., Hanratty, T.J., 1977. Rate of deposition of droplets in annular two-phase flow. Int. J. Multiphase Flow 3, 319–331.

McLaughlin, J.B., 1991. Inertial migration of a small sphere in linear shear flows. J. Fluid Mech. 224, 261–274.

Mei, R., 1992. An approximate expression for the shear lift force on a spherical particle at finite Reynolds number. Int. J. Multiphase Flow 18, 145–147.

Mito, Y., Hanratty, T.J., 2002. Use of a modified Langevin equation to describe turbulent dispersion of fluid particles in a channel flow. Flow Turbulence Combustion 68, 1–26.

Mito, Y., Hanratty, T.J., 2003. A stochastic description of wall sources in a turbulent field: Part 1 Verification. Int. J. Multiphase Flow 29, 1373–1394.

Mito, Y., Hanratty, T.J., 2004. A stochastic description of wall sources in a turbulent field: Part 2. Calculation for a simplified model of horizontal annular flows. Int. J. Multiphase Flow 30, 803–825.

Moser, R.D., Kim, J., Mansour, N.N., 1999. Direct numerical simulation of turbulent channel flow up to $Re_\tau = 590$. Phys. Fluids 11, 943–945.

Na, Y., Papavassiliou, D.V., Hanratty, T.J., 1999. Use of direct numerical simulation to study the effect of Prandtl number on temperature fields. Int. J. Heat Fluid Flow 20, 187–195.

Narayanan, C., Lakehal, D., Botto, L., Soldati, A., 2003. Mechanisms of particle deposition in a fully developed turbulent open channel flow. Phys. Fluids 15, 763–775.

Obukhov, A.M., 1959. Description of turbulence in terms of Lagrangian variables. Adv. Geophys. 6, 113–116.

Ounis, H., Ahmadi, G., McLaughlin, J.B., 1991. Dispersion and deposition of Brownian particles from point sources in a simulated turbulent channel flow. J. Colloid Interface Sci. 147, 233–250.

Pan, L., Hanratty, T.J., 2002a. Correlation of entrainment for annular flow in vertical pipes. Int. J. Multiphase Flow 28, 363–384.

Pan, L., Hanratty, T.J., 2002b. Correlation of entrainment for annular flow in horizontal pipes. Int. J. Multiphase Flow 28, 385–408.

Perkins, R.J., 1992. The entrainment of heavy particles into a plane turbulent jet. Proceedings of the 6th workshop on two-phase flow predictions, Erlangen, ed. M. Sommerfeld, 18–33.

Pozorski, J., Minier, J.P., 1998. On the Lagrangian turbulent dispersion models based on the Langevin equation. Int. J. Multiphase Flow 24, 913–945.

Reeks, M.W., 1977. On the dispersion of small particles suspended in an isotropic turbulent field. J. Fluid Mech. 83, 529–546.

Reeks, M.W., 1983. The transport of discrete particles in inhomogeneous turbulence. J. Aerosol Sci. 14, 729–739.

Reeks, M.W., 2003. Comparison of recent model equations for particle deposition in a turbulent boundary layer with those based on the pdf approach. In: Proceedings of ASME FEDSM'03, Honolulu, USA, Paper No. 45734.

Reeks, M.W., Skyrme, G., 1976. The dependence of particle deposition velocity on particle inertia in turbulent pipe flow. J. Aerosol Sci. 7, 485–495.

Reid, J.D., 1979. Markov chain simulations of vertical dispersion in neutral surface layer for surface and elevated releases. Boundary Layer Meteorol. 16, 3–22.

Reynolds, A.M., 1997. On the application of Thomson's random flight model to the prediction of particle dispersion within a ventilated airspace. J. Wind Eng. Ind. Aerod. 67–68, 627–638.

Saffman, P.G., 1965. The lift on a small sphere in a slow shear flow. J. Fluid Mech. 22, 340–385.

Saffman, P.G., 1968. Corrigendum to The lift on a small sphere in a slow shear flow. J. Fluid Mech. 31, 624.

Shaw, D.A., Hanratty, T.J., 1977. Turbulent mass transfer rates to a wall for large Schmidt numbers. AIChE J. 23, 28–37.

Sommerfeld, M., 2003. Analysis of collision effects for turbulent gas-particle flow in a horizontal channel: Part I. Particle transport. Int. J. Multiphase Flow 29, 675–699.

Sommerfeld, M., Kohnen, G., Rüger, M., 1993. Some open questions and inconsistencies of Lagrangian particle dispersion models. Proceedings of the Ninth Symposium on Turbulent Shear Flows, Kyoto Japan, Paper No. 15–1.

Sun, Y.F., Lin, S.P., 1986. Aerosol concentration in a turbulent flow. J. Colloid Interface Sci. 113, 315–320.

Taylor, G.L., 1921. Diffusion by continuous movements. Proc. London Math. Soc. 20, 196–211.

Thomson, D.J., 1984. Random walk modelling of diffusion in inhomogeneous turbulence. QJR Met. Sci. 110, 1107–1120.

Thomson, D.J., 1986. A random walk model of dispersion in turbulent flows and its application to dispersion in a valley. QJR Met. Sci. 112, 511–530.

Thomson, D.J., 1987. Criteria for the selection of stochastic models of particle trajectories in turbulent flows. J. Fluid Mech. 180, 529–556.

van Dop, H., Nieuwstadt, F.T.M., Hunt, J.C.R., 1985. Random walk models for particle displacements in inhomogeneous unsteady turbulent flows. Phys. Fluids 28, 1639–1653.

van Haarlem, B., Boersma, B.J., Nieuwstadt, F.T.M., 1998. Direct numerical simulation of particle deposition onto a free-slip and no-slip surface. Phys. Fluids 10, 2608–2620.

Wang, Q., Squires, K.D., Chen, M., McLaughlin, J.B., 1997. On the role of the lift force in turbulence simulations of particle deposition. Int. J. Multiphase Flow 23, 749–763.

Wilson, J.D., Thurtell, G.W., Kidd, G.E., 1981. Numerical simulation of particle trajectories in inhomogeneous turbulence, II: Systems with variable turbulent velocity scale. Boundary Layer Meteorol. 21, 423–441.

Woodmansee, D.E., Hanratty, T.J., 1969. Mechanism for the removal of droplets from a liquid surface by a parallel air flow. Chem. Engng. Sci. 24, 299–307.

Yamamoto, Y., Potthoff, M., Tanaka, T., Kajishima, T., Tsuji, Y., 2001. Large-eddy simulation of turbulent gas-particle flow in a vertical channel: effect of considering inter-particle collisions. J. Fluid Mech. 442, 303–334.

Young, J.B., Hanratty, T.J., 1991. Optical studies on the turbulent motion of solid particles in a pipe flow. J. Fluid Mech. 231, 665–688.

Young, J., Leeming, A., 1997. A theory of particle deposition in turbulent pipe flow. J. Fluid Mech. 340, 129–159.

Zhang, H., Ahmadi, G., 2000. Aerosol particle transport and deposition in vertical and horizontal turbulent duct flows. J. Fluid Mech. 406, 55–80.